Alexandria Engineering Journal 118 (2025) 115–124

Contents lists available at ScienceDirect

Alexandria Engineering Journal

journal homepage: www.elsevier.com/locate/aej

Original article

Digital analysis of discrete fractional order cancer model by artificial intelligence

Aziz Khan [a], Thabet Abdeljawad [a,b,c,d,e,i,*], Mahmoud Abdel-Aty [f,g], D.K. Almutairi [h]

[a] Department of Mathematics and Sciences, Prince Sultan University, P.O. Box 66833, 11586 Riyadh, Saudi Arabia
[b] Department of Mathematics, Saveetha School of Engineering, Saveetha Institute of Medical and Technical Sciences, Saveetha University, Chennai 602105, Tamil Nadu, India
[c] Department of Medical Research, China Medical University, Taichung 40402, Taiwan
[d] Center for Applied Mathematics and Bioinformatics (CAMB), Gulf University for Science and Technology, Hawally, 32093, Kuwait
[e] Department of Mathematics and Applied Mathematics, Sefako Makgatho Health Sciences University, Garankuwa, Medusa 0204, South Africa
[f] Deanship of Graduate Studies and Research, Ahlia University, P.O. Box 10878, Manama, Kingdom of Bahrain
[g] Abu Dhabi University, Zayed City, MZ39, Abu Dhabi, United Arab Emirates
[h] Department of Mathematics, College of Science Al-Zulfi, Majmaah University, 11952 Al-Majmaah, Saudi Arabia
[i] Department of Mathematics, Kyung Hee University 26 Kyungheedae-ro, Dongdaemun-gu, 02447 Seoul, Korea

ARTICLE INFO

Keywords:
Discrete fractional order Caputo Cancer model
Iterative numerical method
Neural networks
Bayesian regularization
Training state

ABSTRACT

This article presents the approximate numerical solutions of the novel constructed Difference Caputo Order Cancer (DCOC) model utilizing the iterative numerical method combined with the neural network approach. The DCOC model is systemized for five variables and is further classified into four stages for investigation. Various fractional orders are considered to study the different scenarios of the DCOC model. The iterative systems of the DCOC model have been formulated by the iterative numerical method with neural networks associated with the computational operation of the Bayesian Regularization (BR), referred to as ENNs-BR. All the results of the DCOC model are compared by their performance. For the statistical study, the data of the model considered is partitioned into 75% and 25% in two parts. Finally, the results for performance, training state, error histogram, regression, and fit are illustrated graphically.

1. Introduction

Breast cancer, one of the most predominant types of cancer affecting women globally, is indicated by four distinct stages that reveal the extent of its development and spread within the body [1]. Each stage characterizes a different level of severity and manages treatment based on factors such as metastasis, tumor size, and lymph node involvement [2]. In the first stage, known as carcinoma in situ, the cancerous cells are restricted to the lobules or ducts of the breast tissue and have not infected surrounding healthy tissue. This stage is often proposed non-invasive and highly treatable with surgery, such as mastectomy or lumpectomy to eliminate the abnormal cells. In the second stage, breast cancer indicates that the tumor is quite small, less than 2 centimeters in diameter, and has not spread elsewhere in the breast. It may or may not contain nearby lymph nodes. Treatment typically includes surgery keep on by chemotherapy or radiation therapy to eliminate any remaining cancer cells and decrease the risk of return [3]. In the third stage, the cancer is a tumor between 2 to 5 centimeters or has spread to near lymph nodes. This stage is divided into Stage 2A and Stage 2B based on the size of the tumor and level of lymph node envelopment. Treatment decisions may contain a combination of radiation therapy, surgery, targeted therapy, and chemotherapy, personalized to the particular features of the tumor and the individual patient. In the third stage, breast cancer is measured as locally advanced, where the tumor is larger and may have spread more lengthily to nearby lymph nodes and tissues, such as the chest wall or skin. We can see Fig. 1, different affecting areas of the breast.

This stage is further considered into stages 3A, 3B, and 3C based on the extent of tumor size and lymph node involvement [5]. Treatment typically contains a combination of chemotherapy, radiation therapy, surgery, and targeted therapy to shrink the tumor and control its spread. In 4th stage, breast cancer, also known as metastatic breast

* Corresponding author.
E-mail addresses: akhan@psu.edu.sa (A. Khan), tabdeljawad@psu.edu.sa (T. Abdeljawad), amisaty@gmail.com (M. Abdel-Aty), dk.almutairi@mu.edu.sa (D.K. Almutairi).

https://doi.org/10.1016/j.aej.2025.01.036
Received 7 October 2024; Received in revised form 4 December 2024; Accepted 7 January 2025
Available online 21 January 2025

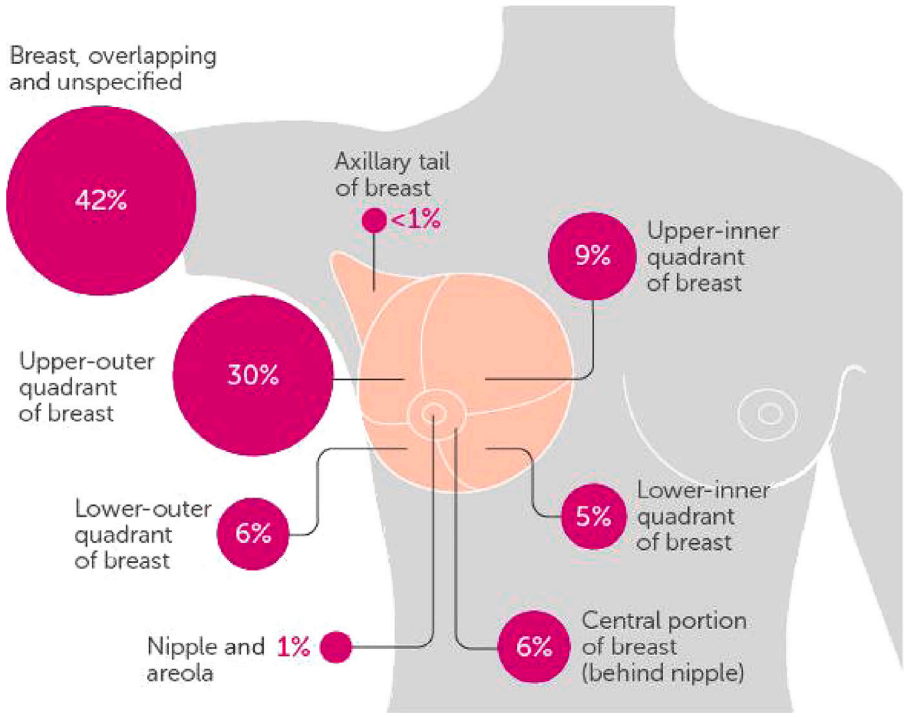

Fig. 1. Different effecting zones [4].

cancer, shows that the cancer has spread beyond the breast and nearby lymph nodes to other organs of the body, such as the lungs, liver, bones, or brain [6]. This stage is considered advanced and incurable, fixing on managing symptoms, refining the quality of life, and extending survival through systemic treatments like targeted therapy, chemotherapy, occasionally surgery or radiation, and hormonal therapy to control the disease's progression [7].

Mathematical modeling of breast cancer has occurred as a pivotal tool in understanding the complex mechanisms fundamental to its response to treatment, progression, and development [8]. These models employ mathematical equations to study the biological processes particular to breast cancer, including factors such as genetic mutations, tumor growth kinetics, interactions, and hormone receptor status with the immune system [9]. By computing these variables, mathematical models deliver insights into tumor dynamics over time, from the original stages of tumor construction to metastasis [10]. For example, compartmental models classify breast cancer into distinct parts based on disease stages and biological characteristics, enabling the study of disease progress and treatment consequences. Benzekry et al. [11] presented computational simulations for effectively curbing primary tumor growth but showed limited efficacy in removing micrometastatic disease progression after surgery and treatment cessation. Different machine learning approaches, counting support vector machines, random forests, and artificial neural networks, complete the absence of definitive biomarkers, underscoring the importance of preclinical modeling to expect potential clinical limitations and enhance treatment strategies.

A fractional-order cancer model incorporates principles of fractional calculus better to understand the dynamics of cancer growth and treatment response. This technique recognizes the non-integer order derivatives that illustrate complex biological systems and presents a more nuanced view related to traditional integer-order models. By including fractional operators, the model presents the memory and hereditary properties inherent in biological models, giving details for more accurate predictions of tumor growth and response to therapies. Artificial intelligence (AI) and neural networking techniques improve the model's predictive power by optimizing estimation and simulating complex dealings within the tumor microenvironment. Neural networks, specifically, aid in processing large datasets and classifying patterns that may not seem through conservative methods, thereby refining the model's accuracy in predicting treatment results and considering the fundamental mechanisms of cancer progression. Combining AI and neural networking with fractional-order cancer models helps tailor medicine approaches, modifying treatments based on different patient types and tumor behavior. This approach holds promise for progressing cancer research and therapy development, potentially important to more effective treatments and developed patient results in the future. Arshad et al. [12] used the Laplace Variational Iterational technique to study the complex behavior of the cancer model with chemotherapy treatment. The results obtained were illustrated by graphs. Chavada et al. [13] presented a cancer model with smoking considered with fractional-order designed with seven variables. The Adams–Bashforth–Moulton technique was employed for the numerical results and the existence solution of the model was obtained by Banach's fixed-point approach. Finally, stability is discussed by Hyers–Ulam criterion. The results were expressed in 2D and 3D graphs for various fractional orders, combined with parameters. Mohammadpoor et al. [14] studied the breast cancer model with chemotherapy by considering the model in the Caputo–Fabrizio operator. Hyers–Ulam stability was used for stability analysis. Numerical visualization is presented for all compartments of the model. Aldwoah et al. [15] presented the breast cancer model by considering the model in the ABC fractional operator. The stability of the model was investigated by Hyers–Ulam stability. The obtained results were graphically demonstrated. For more details see [16–21]. This article, organized in such way given in Fig. 2,

- This article deals with numerical approximate solutions for the newly constructed DCOC model employing an iterative numerical method associated with neural networks.

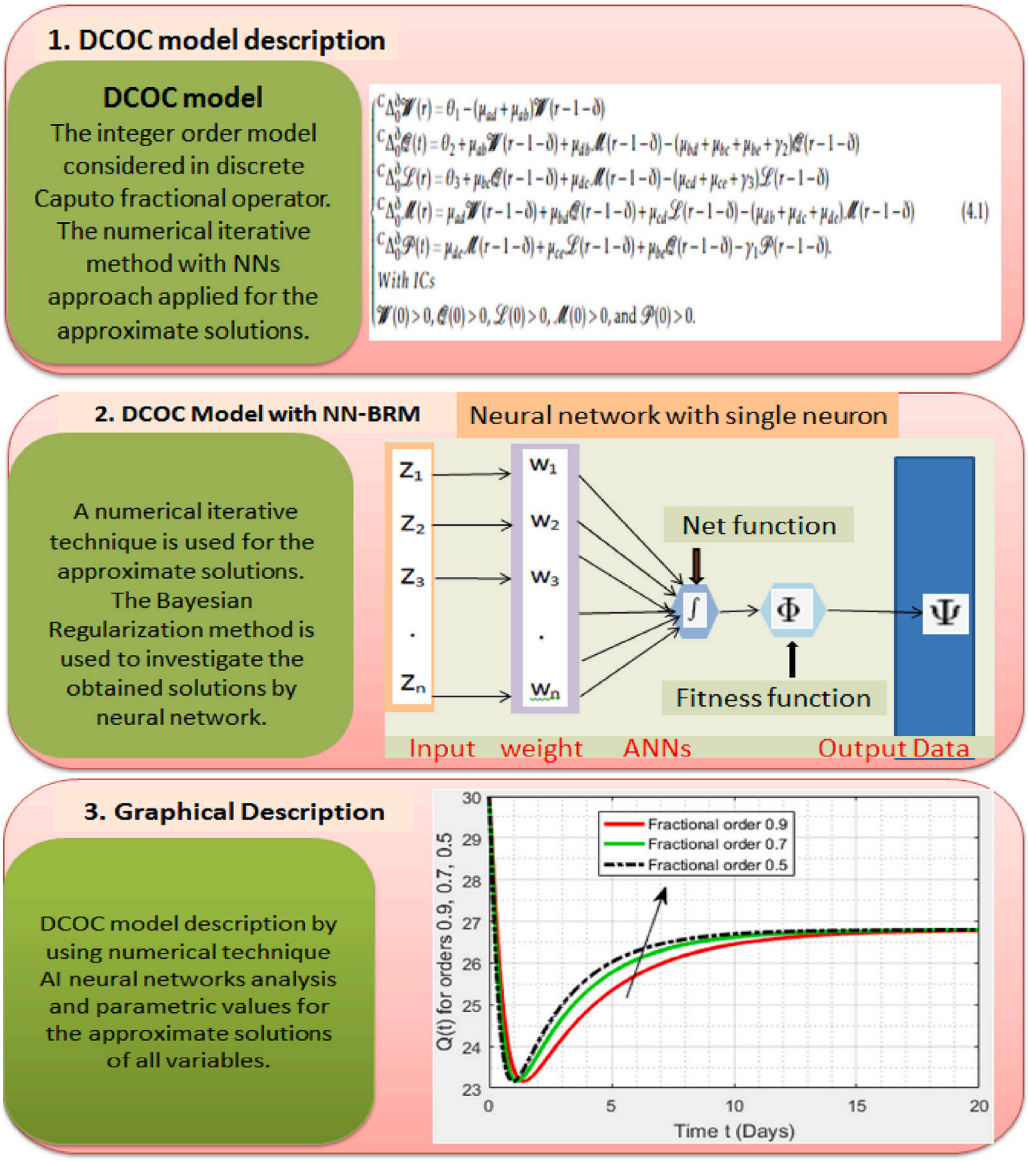

Fig. 2. Flow chart article organization.

- The DCOC model is formulated with five variables and three cases with different fractional order has been investigated for dynamical behavior.
- An iterative method for the DCOC model, denoted as ENNs-BR, is developed utilizing the iterative numerical technique with neural networks and the Bayesian Regularization (BR).
- Performance of the model is investigated by partitioned the obtained data into 75% training and 25% testing, with graphical demonstration provided for fit, performance, regression, training state, and error histogram.

2. Preliminaries results

This section introduces the basic definitions and main concepts correlated to fractional sum and difference operators. It is desirable to consult the recommended resources for more thorough knowledge, which propound detailed clarifications and widespread information on these topics. Can be found here [22–26].

The Caputo-like difference operator ${}^{C}\Delta_0^{\delta}\Psi(r)$ of a function $\Psi(r)$ is characterized as:

$$ {}^{C}\Delta_0^{\delta}\Psi(r) = \Delta_0^{-(1-\delta)}\Delta\Psi(t) = \frac{1}{\Gamma(1-\delta)}\sum_{t=0}^{r-(1-\delta)}(r-1-t)^{-\delta}\Delta\Psi(t). $$

Here, $\Delta_0^{-\delta}$ is the δ-th fractional sum, which is formulated as:

$$ \Delta_0^{-\delta}\Psi(z) = \frac{1}{\Gamma(\delta)}\sum_{z=0}^{r-\delta}(r-1-z)^{(\delta-1)}\Psi(z), $$

with $\delta > 0$. The term $(r-1-z)^{(\delta-1)}$ denotes the falling function, which is defined as:

$$ (r-1-z)^{(\delta-1)} = \frac{\Gamma(r-z)}{\Gamma(r-z-\delta+1)}. $$

3. Model DCOC formulation

The DCOC model formulated for breast cancer [27–29]. This model is constructed for five classes of breast cancer patients. Each class is denotes by $\mathscr{W}, \mathscr{Q}, \mathscr{L}, \mathscr{M}$, and $\mathscr{P}$ variables in the model. The class $\mathscr{W}$ denotes patients effected of cancer, stage 1, $2\mathscr{W}$, and $2\mathscr{Q}$. The class $\mathscr{Q}$ represents patients at stage $3\mathscr{W}$ and $2\mathscr{Q}$. The class $\mathscr{L}$ denotes cancer patients at stage 4. The class $\mathscr{M}$ cancer patients with chemotherapy stage. With disease-free, with no cancer. The class $\mathscr{P}$ cancer patients with cardiotoxicity.

$$\begin{cases} {}^{C}\Delta_0^{\eth}\mathscr{W}(r) = \theta_1 - (\mu_{ad}+\mu_{ab})\mathscr{W}(r-1-\eth) \\ {}^{C}\Delta_0^{\eth}\mathscr{Q}(t) = \theta_2 + \mu_{ab}\mathscr{W}(r-1-\eth) + \mu_{db}\mathscr{M}(r-1-\eth) \\ \qquad -(\mu_{bd}+\mu_{bc}+\mu_{be}+\gamma_2)\mathscr{Q}(r-1-\eth) \\ {}^{C}\Delta_0^{\eth}\mathscr{L}(r) = \theta_3 + \mu_{bc}\mathscr{Q}(r-1-\eth) + \mu_{dc}\mathscr{M}(r-1-\eth) \\ \qquad -(\mu_{cd}+\mu_{ce}+\gamma_3)\mathscr{L}(r-1-\eth) \\ {}^{C}\Delta_0^{\eth}\mathscr{M}(r) = \mu_{ad}\mathscr{W}(r-1-\eth) + \mu_{bd}\mathscr{Q}(r-1-\eth) + \mu_{cd}\mathscr{L}(r-1-\eth) \\ \qquad -(\mu_{db}+\mu_{dc}+\mu_{de})\mathscr{M}(r-1-\eth) \\ {}^{C}\Delta_0^{\eth}\mathscr{P}(t) = \mu_{de}\mathscr{M}(r-1-\eth) + \mu_{ce}\mathscr{L}(r-1-\eth) \\ \qquad +\mu_{be}\mathscr{Q}(r-1-\eth) - \gamma_1\mathscr{P}(r-1-\eth). \\ With\ \ ICs \\ \mathscr{W}(0)>0, \mathscr{Q}(0)>0, \mathscr{L}(0)>0, \mathscr{M}(0)>0, and \mathscr{P}(0)>0. \end{cases} \tag{3.1}$$

For $r \in \mathbb{N}^{1-\eth}$, where $\mathbb{N}^{1-\eth} = \{1-\eth, 2-\eth, 3-\eth, \dots\}$, $0 < \eth_j \le 1$, $j = 1,2,3$ denotes fractional orders. The Caputo difference operator ${}^{C}\Delta_0^{\eth}\Phi(r)$. Where, all the parameters of the model are defined as, θ_1 the new patients whose are at stage 1 and 2 diagnosed, θ_2 patients at stage 3 diagnosed, θ_3, patients diagnosed at stage 4 diagnosed, increased rate μ_{ab} at stage 1 or 2 with 3, the rate of patients μ_{ad} at stage 1 or 2, the rate μ_{bd} at stage 3, the rate μ_{bc} at stage 3 to stage 4, the rat of patients μ_{be} at stage 3 with chemotherapy who experience cardiotoxic, the rate μ_{cd} at stage 4 with experience complete response, the rate μ_{ce} at stage 4 with chemotherapy patients who experience cardiotoxic, The rate μ_{bd} of patients disease-free at stage 3, the rate μ_{dc} patients of disease-free relapse back at stage 4, the rate μ_{de} patients disease-free with experience cardiotoxic, the death rate γ_1 of cardiotoxic patients, the death rate γ_2 at stage 3 cancer, the death rate γ_3 at stage 4.

4. Numerical scheme of DCOC model

In this context, the DCOC model, using the Caputo fractional order, is numerically investigated using first-order convergent numerical techniques as given in [30,31]. These techniques are known for their accuracy, convergence, and conditional stability when operated on linear or nonlinear fractional-order models.

Consider a delta difference system having an autonomous nature:

$${}^{C}\Delta_a^{\eth_i}\Psi(r) = g(r+\eth_i-1, y(r+\eth_i-1)) \tag{4.1}$$

$$\Delta^m\Psi(r) = \psi_m, \quad z = \lceil \eth_i \rceil + 1, \quad m = 0,1,\dots,z-1, \quad i = 1,2,3,4,5. \tag{4.2}$$

The unique solution of this initial value problem (3.1) is given by:

$$\Psi(r) = \Psi_0(r) + \frac{1}{\Gamma(\eth_i)} \sum_{\tau=a+z-\eth_i}^{r-\eth_i} (r-\sigma(\tau))^{\eth_i-1} g(\tau+\eth_i-1, \Psi(\tau+\eth_i-1)), \quad r \in N_{a+z}, \tag{4.3}$$

where

$$\Psi_0(r) = \sum_{m=0}^{z-1} \frac{(r-a)^m}{\Gamma(m+1)} \Delta^m\Psi(a). \tag{4.4}$$

where $\Psi = (\upsilon 1, \upsilon 2, \upsilon 3, \upsilon 4, \upsilon 5) \in \mathrm{R}_+^5$ is a real-valued continuous vector function. The $\Delta_0^{-\eth}$ fractional-order sum operator. By considering equally spaced integration intervals over $[0,T]$ with a fixed step size h, for the simulation), where $h = \frac{T}{n}$ and $n \in \mathbb{N}$, we approximate $\Psi(r)$ at $t = t_q$ for $q = 0,1,\dots,n$. Let

$$\begin{cases} \Xi_1 = \theta_1 - (\mu_{ad}+\mu_{ab})\mathscr{W}(r-1-\eth) \\ \Xi_2 = \theta_2 + \mu_{ab}\mathscr{W}(r-1-\eth) + \mu_{db}\mathscr{M}(r-1-\eth) - (\mu_{bd}+\mu_{bc}+\mu_{be} \\ \qquad +\gamma_2)\mathscr{Q}(r-1-\eth) \\ \Xi_3 = \theta_3 + \mu_{bc}\mathscr{Q}(r-1-\eth) + \mu_{dc}\mathscr{M}(r-1-\eth) \\ \qquad -(\mu_{cd}+\mu_{ce}+\gamma_3)\mathscr{L}(r-1-\eth) \\ \Xi_4 = \mu_{ad}\mathscr{W}(r-1-\eth) + \mu_{bd}\mathscr{Q}(r-1-\eth) + \mu_{cd}\mathscr{L}(r-1-\eth) \\ \qquad -(\mu_{db}+\mu_{dc}+\mu_{de})\mathscr{M}(r-1-\eth) \\ \Xi_5 = \mu_{de}\mathscr{M}(r-1-\eth) + \mu_{ce}\mathscr{L}(r-1-\eth) + \mu_{be}\mathscr{Q}(r-1-\eth) \\ \qquad -\gamma_1\mathscr{P}(r-1-\eth). \end{cases} \tag{4.5}$$

The numerical scheme for the DCOC model by the Caputo fractional operator is given by:

$$\mathscr{W}(r) = \mathscr{W}(0) + \frac{1}{\Gamma(\eth)} \sum_{j=0}^{r-1} \frac{\Gamma(r-j-1+\eth)}{\Gamma(r-j)} \Xi_1,$$

$$\mathscr{Q}(r) = \mathscr{Q}(0) + \frac{1}{\Gamma(\eth)} \sum_{j=0}^{r-1} \frac{\Gamma(r-j-1+\eth)}{\Gamma(r-j)} \Xi_2,$$

$$\mathscr{L}(r) = \mathscr{L}(0) + \frac{1}{\Gamma(\eth)} \sum_{j=0}^{r-1} \frac{\Gamma(r-j-1+\eth)}{\Gamma(r-j)} \Xi_3,$$

$$\mathscr{M}(r) = \mathscr{M}(0) + \frac{1}{\Gamma(\eth)} \sum_{j=0}^{r-1} \frac{\Gamma(r-j-1+\eth)}{\Gamma(r-j)} \Xi_4,$$

$$\mathscr{P}(r) = \mathscr{P}(0) + \frac{1}{\Gamma(\eth)} \sum_{j=0}^{r-1} \frac{\Gamma(r-j-1+\eth)}{\Gamma(r-j)} \Xi_5.$$

The discrete difference sense suggests that we are analyzing the differences between consecutive terms in the sequences, multiplied by the fractional power terms. This supports with the discrete construction of fractional calculus where sums substitute integrals and finite differences replace operators.

We now discuss the numerical results obtained for the model concerning the approximate solutions. To achieve this, we utilized the efficient Euler method under the Caputo fractional operator.

5. Analysis by artificial intelligence of DCOC model

The analysis of discrete fractional order cancer models in the sense of the Caputo operator has taken a momentous leap forward with the use of artificial intelligence neural networking. By leveraging the Caputo operator, researchers can efficiently handle the complexities connected with fractional calculus, which is important in accurately modeling the irregular diffusion and various behaviors observed in cancer dynamics [32–42]. The integration of AI neural networks Fig. 4, into this structure offers a powerful tool for improving the model's predictive capabilities. Neural networks, with their facility to learn from large datasets and recognize intricate patterns, afford a sophisticated means to examine and predict the progression of cancer with high accuracy. In this study, the discrete fractional cancer model established and trained exhausting neural networks to approximate the behavior of cancer cells under numerous conditions. The Caputo operator is associated with the discrete operator, providing a more precise mathematical demonstration of the cancer dynamics assessed to traditional integer-order models. The neural network was trained on a dataset comprising different parameters important to cancer progression, such as cell proliferation rates, mutation frequencies, and treatment responses. The dataset was distributed into 75% for training and 25% for testing to guarantee a robust validation of the model (see Figs. 4 and 7).

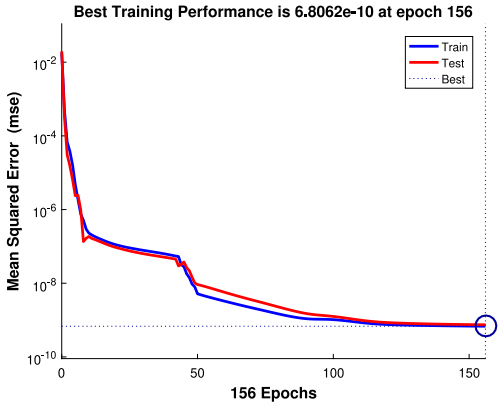

(a) For Case 1: MSE performance for epochs 156 of the model (6.1).

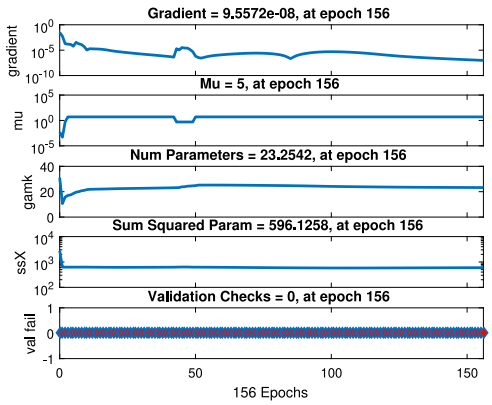

(b) For Case 1: training test for epochs 156 of the model (6.1).

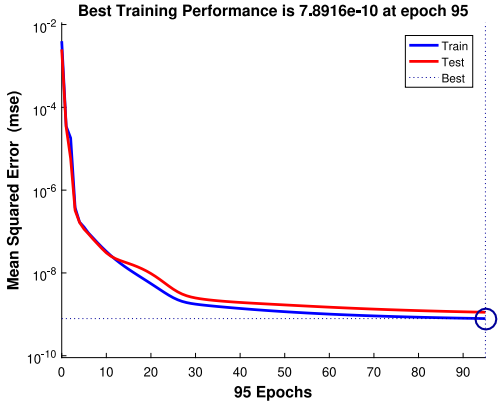

(c) For Case 2: MSE performance for epochs 95 of the model (6.2).

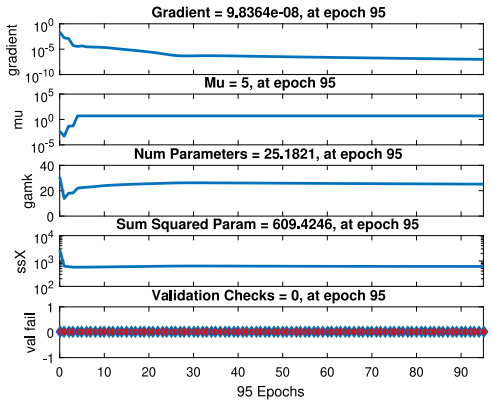

(d) For Case 2: training test for epochs 95 of the model (6.2).

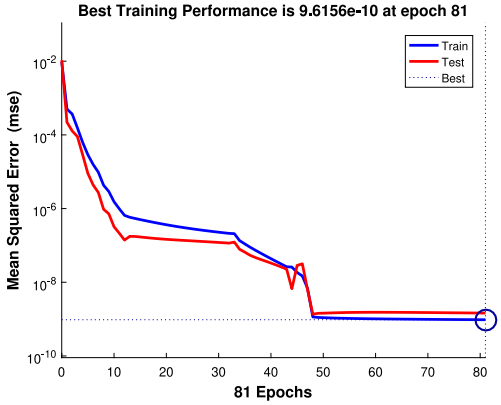

(e) For Case 3: MSE performance for epochs 81 of the model (6.3).

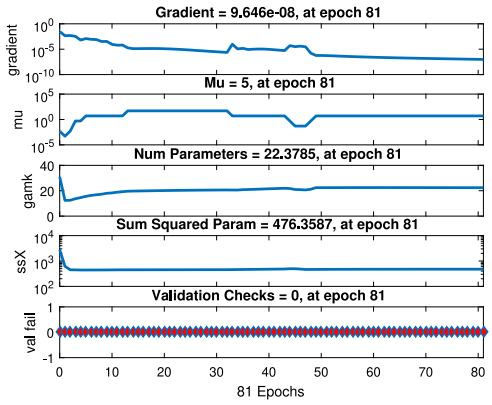

(f) For Case 3: training test for epochs 81 of the model (6.3).

Fig. 3. MSE and training test illustration for different fractional order of the DCOC model (3.1).

In Fig. 3, we investigate MSEs and training tests for Case 1, Case 2, and Case 3 for different fractional orders of the DCOC model (3.1). In Fig. 5, we investigate training fit and training histogram for Case 1, Case 2, and Case 3 for different fractional orders of the DCOC model (3.1). In Fig. 6, we investigate training regression for Case 1, Case 2, and Case 3 for different fractional orders of the DCOC model (3.1). The

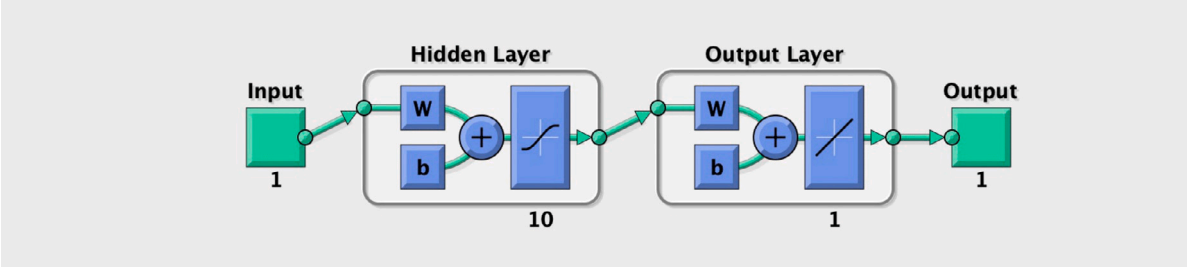

(a)

Fig. 4. Neural network of the system (3.1), FFPPV model.

neural network's performance was assessed using numerous metrics, containing mean squared error, regression analysis, and model fit assessment. Error histograms are produced to visualize the distribution of prediction errors, emphasizing the model's accuracy and areas for prospective improvement. Regression investigations provided visions of the relationship between predicted and actual results, while training states and model fit calculations offered a comprehensive estimation of the neural network's learning process. One of the key benefits of consuming neural networks in this framework is their ability to handle non-linearities and complex relations within the data, which are common in cancer progression. The neural network's architecture deliberates in capturing these complexities, with multiple layers and stimulation functions tailored to optimize performance. Moreover, regularization methods check overfitting, guaranteeing that the model generalizes well to new, unseen data.

6. Numerical discussion of DCOC model

We considered the DCOC model to study their dynamics in the fractional derivate, we developed a numerical scheme for the approximate results. For different fractional orders, we check the dynamical behavior of the Eq. (3.1) , DCOC model. The graphs Fig. 7, show that the fractional order behaves like an integer order and closely goes. By utilizing the variable class values and parametric values we see the graphs. Three cases for the fractional order discussed **Case:1** The impact of $\eth_1, = 0.9$, on the $\mathscr{W}, \mathscr{Q}, \mathscr{L}, \mathscr{M}$, and $\mathscr{P}$ classes, of the DCOC model. Using the parametric values of the suggested model. such, $\theta_1 = 14000, \theta_3 = 90, \mu_{ab} = 0.034, \mu_{dc} = 0.3, \mu_{ce} = 0.1, \gamma_1 = 0.0256, \gamma_3 = 0.0256, \mu_{bd} = 0.4, \theta_2 = 0.80, \mu_{bc} = 0.01, \mu_{ad} = 0.03, \mu_{be} = 0.03, \mu_{de} = 0.2, \gamma_2 = 0.0256, \mu_{dc} = 0.03, \mu_{cd} = 0.01$, and with initial values $(\mathscr{W} = 30000, \mathscr{Q} = 12300, \mathscr{L} = 783, \mathscr{M} = 334, \mathscr{P} = 11)$.

$$\begin{cases} {}^{C}\Delta_0^{\eth_1}\mathscr{W}(r) = \theta_1 - (\mu_{ad} + \mu_{ab})\mathscr{W}(r-1-\eth_1) \\ {}^{C}\Delta_0^{\eth_1}\mathscr{Q}(r) = \theta_2 + \mu_{ab}\mathscr{W}(r-1-\eth_1) + \mu_{db}\mathscr{M}(r-1-\eth_1) \\ \qquad -(\mu_{bd} + \mu_{bc} + \mu_{be} + \gamma_2)\mathscr{Q}(r-1-\eth_1) \\ {}^{C}\Delta_0^{\eth_1}\mathscr{L}(r) = \theta_3 + \mu_{bc}\mathscr{Q}(r-1-\eth_1) + \mu_{dc}\mathscr{M}(r-1-\eth_1) \\ \qquad -(\mu_{cd} + \mu_{ce} + \gamma_3)\mathscr{L}(r-1-\eth_1) \\ {}^{C}\Delta_0^{\eth_1}\mathscr{M}(r) = \mu_{ad}\mathscr{W}(r-1-\eth_1) + \mu_{bd}\mathscr{Q}(r-1-\eth_1) + \mu_{cd}\mathscr{L}(r-1-\eth_1) \\ \qquad -(\mu_{db} + \mu_{dc} + \mu_{de})\mathscr{M}(r-1-\eth_1) \\ {}^{C}\Delta_0^{\eth_1}\mathscr{P}(t) = \mu_{de}\mathscr{M}(r-1-\eth_1) + \mu_{ce}\mathscr{L}(r-1-\eth_1) \\ \qquad +\mu_{be}\mathscr{Q}(r-1-\eth_1) - \gamma_1\mathscr{P}(r-1-\eth_1). \end{cases} \tag{6.1}$$

Case:2 The impact of $\eth_2, = 0.7$, on the $\mathscr{W}, \mathscr{Q}, \mathscr{L}, \mathscr{M}$, and $\mathscr{P}$ classes, of the DCOC model. Using the parametric values of the suggested model. such, $\theta_1 = 14000, \theta_3 = 90, \mu_{ab} = 0.034, \mu_{dc} = 0.3, \mu_{ce} = 0.1, \gamma_1 = 0.0256, \gamma_3 = 0.0256, \mu_{bd} = 0.4, \theta_2 = 0.80, \mu_{bc} = 0.01, \mu_{ad} = 0.03, \mu_{be} = 0.03, \mu_{de} = 0.2, \gamma_2 = 0.0256, \mu_{dc} = 0.03, \mu_{cd} = 0.01$, and with initial values $(\mathscr{W} = 30000, \mathscr{Q} = 12300, \mathscr{L} = 783, \mathscr{M} = 334, \mathscr{P} = 11)$.

$$\begin{cases} {}^{C}\Delta_0^{\eth_2}\mathscr{W}(r) = \theta_2 - (\mu_{ad} + \mu_{ab})\mathscr{W}(r-1-\eth_2) \\ {}^{C}\Delta_0^{\eth_2}\mathscr{Q}(r) = \theta_2 + \mu_{ab}\mathscr{W}(r-1-\eth_2) + \mu_{db}\mathscr{M}(r-1-\eth_2) \\ \qquad -(\mu_{bd} + \mu_{bc} + \mu_{be} + \gamma_2)\mathscr{Q}(r-1-\eth_2) \\ {}^{C}\Delta_0^{\eth_2}\mathscr{L}(r) = \theta_3 + \mu_{bc}\mathscr{Q}(r-1-\eth_2) + \mu_{dc}\mathscr{M}(r-1-\eth_2) \\ \qquad -(\mu_{cd} + \mu_{ce} + \gamma_3)\mathscr{L}(r-1-\eth_2) \\ {}^{C}\Delta_0^{\eth_2}\mathscr{M}(r) = \mu_{ad}\mathscr{W}(r-1-\eth_2) + \mu_{bd}\mathscr{Q}(r-1-\eth_2) + \mu_{cd}\mathscr{L}(r-1-\eth_2) \\ \qquad -(\mu_{db} + \mu_{dc} + \mu_{de})\mathscr{M}(r-1-\eth_2) \\ {}^{C}\Delta_0^{\eth_2}\mathscr{P}(t) = \mu_{de}\mathscr{M}(r-1-\eth_2) + \mu_{ce}\mathscr{L}(r-1-\eth_2) \\ \qquad +\mu_{be}\mathscr{Q}(r-1-\eth_2) - \gamma_1\mathscr{P}(r-1-\eth_2). \end{cases} \tag{6.2}$$

Case:3 The impact of $\eth_3, = 0.5$, on the $\mathscr{W}, \mathscr{Q}, \mathscr{L}, \mathscr{M}$, and $\mathscr{P}$ classes, of the DCOC model. Using the parametric values of the suggested model. such, $\theta_1 = 14000, \theta_3 = 90, \mu_{ab} = 0.034, \mu_{dc} = 0.3, \mu_{ce} = 0.1, \gamma_1 = 0.0256, \gamma_3 = 0.0256, \mu_{bd} = 0.4, \theta_2 = 0.80, \mu_{bc} = 0.01, \mu_{ad} = 0.03, \mu_{be} = 0.03, \mu_{de} = 0.2, \gamma_2 = 0.0256, \mu_{dc} = 0.03, \mu_{cd} = 0.01$, and with initial values $(\mathscr{W} = 30000, \mathscr{Q} = 12300, \mathscr{L} = 783, \mathscr{M} = 334, \mathscr{P} = 11)$.

$$\begin{cases} {}^{C}\Delta_0^{\eth_3}\mathscr{W}(r) = \theta_2 - (\mu_{ad} + \mu_{ab})\mathscr{W}(r-1-\eth_3) \\ {}^{C}\Delta_0^{\eth_3}\mathscr{Q}(r) = \theta_2 + \mu_{ab}\mathscr{W}(r-1-\eth_2) + \mu_{db}\mathscr{M}(r-1-\eth_3) \\ \qquad -(\mu_{bd} + \mu_{bc} + \mu_{be} + \gamma_3)\mathscr{Q}(r-1-\eth_2) \\ {}^{C}\Delta_0^{\eth_3}\mathscr{L}(r) = \theta_3 + \mu_{bc}\mathscr{Q}(r-1-\eth_3) + \mu_{dc}\mathscr{M}(r-1-\eth_3) \\ \qquad -(\mu_{cd} + \mu_{ce} + \gamma_3)\mathscr{L}(r-1-\eth_3) \\ {}^{C}\Delta_0^{\eth_3}\mathscr{M}(r) = \mu_{ad}\mathscr{W}(r-1-\eth_2) + \mu_{bd}\mathscr{Q}(r-1-\eth_3) + \mu_{cd}\mathscr{L}(r-1-\eth_3) \\ \qquad -(\mu_{db} + \mu_{dc} + \mu_{de})\mathscr{M}(r-1-\eth_3) \\ {}^{C}\Delta_0^{\eth_3}\mathscr{P}(t) = \mu_{de}\mathscr{M}(r-1-\eth_3) + \mu_{ce}\mathscr{L}(r-1-\eth_3) \\ \qquad +\mu_{be}\mathscr{Q}(r-1-\eth_2) - \gamma_1\mathscr{P}(r-1-\eth_3). \end{cases} \tag{6.3}$$

7. Conclusion

This work studied DCOC and the numerical iterative technique utilized to analyze the obtained results with different fractional orders. This study proposes a quick approximation approach to the discrete fractional cancer model by using the Caputo operator. Further, comparing outcomes for different orders evaluates their performance by artificial intelligence. Performance metrics contain error histograms, regression analyses, training states, and model fit assessments. For statistical data, the dataset utilized in the study is divided into 75% for training functions and 25% for testing. In Fig. 3, we studied MSEs and training tests for Case 1, Case 2, and Case 3 for different fractional orders of the DCOC model (3.1). In Fig. 5, we investigated training fit and training histogram for Case 1, Case 2, and Case 3 for different

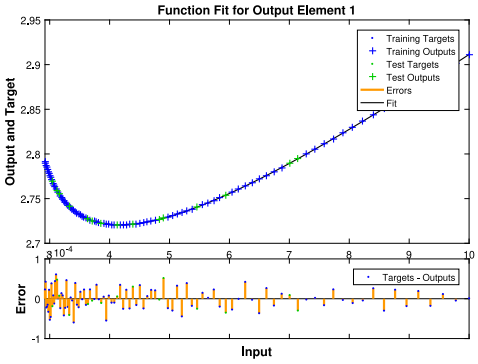

(a) For Case 1: Training fit for epochs 156 of the model (6.1).

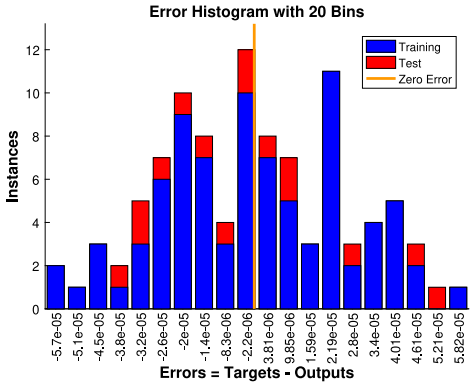

(b) For Case 2: training histogram for epochs 156 of the model (6.1).

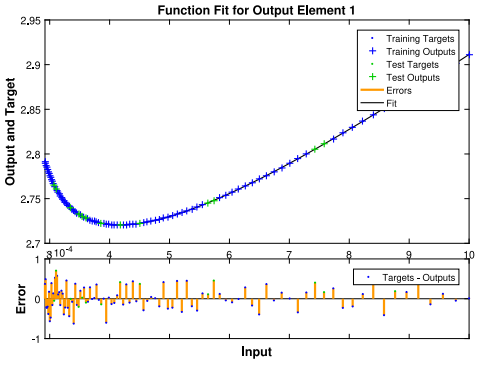

(c) For Case 2: Training fit for epochs 95 of the model (6.2).

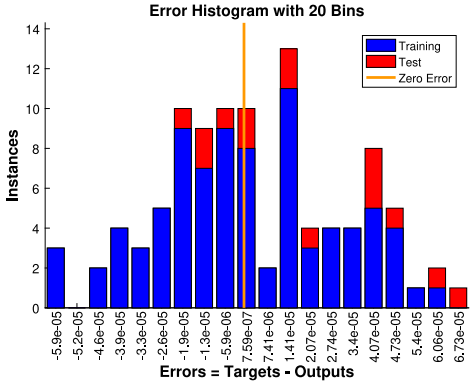

(d) For Case 3: training histogram for epochs 95 of the model (6.2).

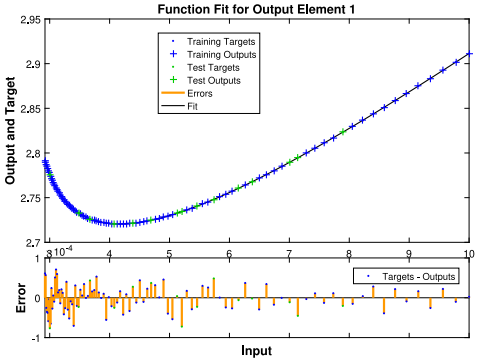

(e) For Case 1: Training fit for epochs 81 of the model (6.3).

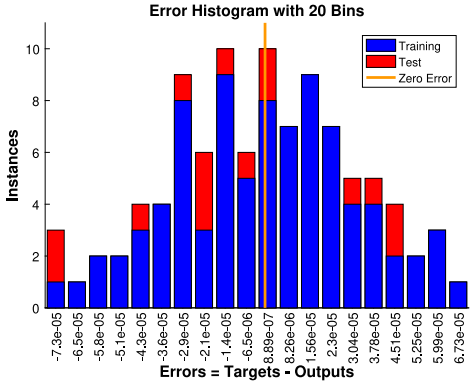

(f) For Case 3: training histogram for epochs 81 of the model (6.3).

Fig. 5. Training fit and histogram training for different fractional order of the DCOC model (3.1).

fractional orders of the DCOC model (3.1). In Fig. 6, we examined training regression for Case 1, Case 2, and Case 3 for different fractional orders of the DCOC model (3.1). This splitting ensures robust estimation of the model's predictive competencies.

Future research directions could include exploring alternative fractional operators and including more complex datasets to further confirm and enhance the model's capabilities. Furthermore, researchers might examine the impact of varying the training and testing data

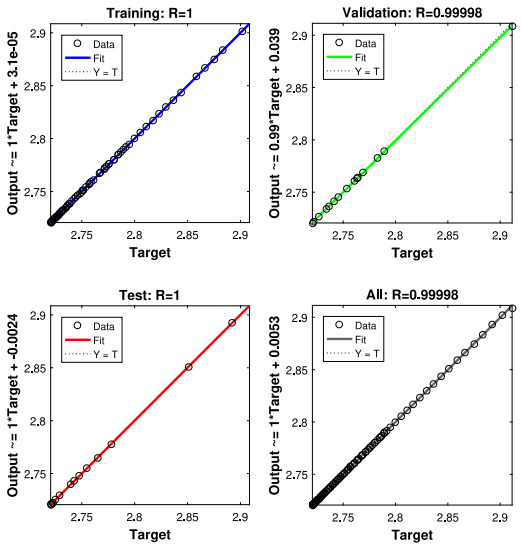

(a) For Case 1: training regression for epochs 156 of the model (6.1).

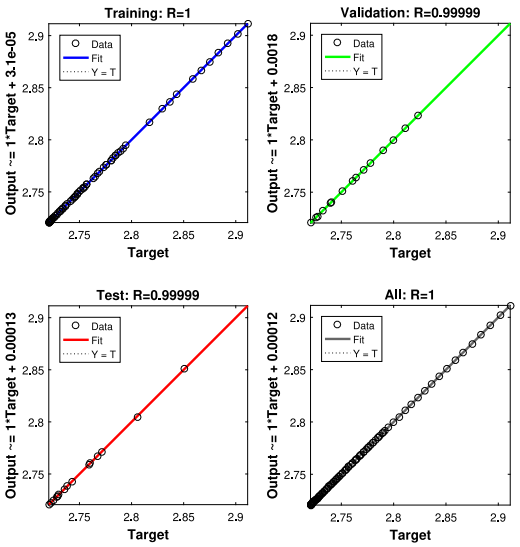

(b) For Case 2: training regression for epochs 95 of the model (6.2).

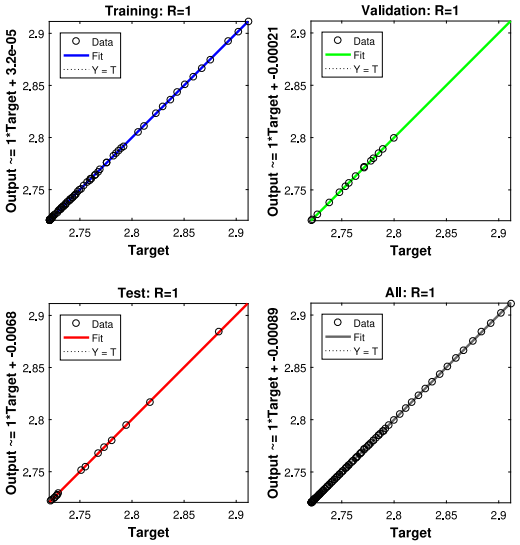

(c) For Case 3: training regression for epochs 81 of the model (6.3).

Fig. 6. Training regression for different fractional order of the DCOC model (3.1).

proportions to establish the optimal split for different types of datasets. Developing the model to contain multi-dimensional data could also afford deeper insights into its applicability in real-world scenarios. Another potential area of investigation is the development of hybrid models that combine the Caputo operator with another numerical method to improve accuracy and efficiency. By concentrating on these avenues, future researchers can build on the foundational work obtainable here, evolving the understanding and application of discrete fractional cancer models without depending on AI-generated content. This approach will lead to the development of more sophisticated and reliable analytical mathematical models in the field of cancer research, ultimately supporting the early detection and treatment of the disease.

CRediT authorship contribution statement

Aziz Khan: Writing – original draft, Methodology, Conceptualization. **Thabet Abdeljawad:** Supervision, Investigation. **Mahmoud Abdel-Aty:** Visualization. **D.K. Almutairi:** Formal analysis.

Declaration of competing interest

The authors declare that there is no conflict of interests regarding the publication of this paper.

Acknowledgments

D.K.A. extends the appreciation to the Deanship of Postgraduate Studies and Scientific Research at Majmaah University for funding this

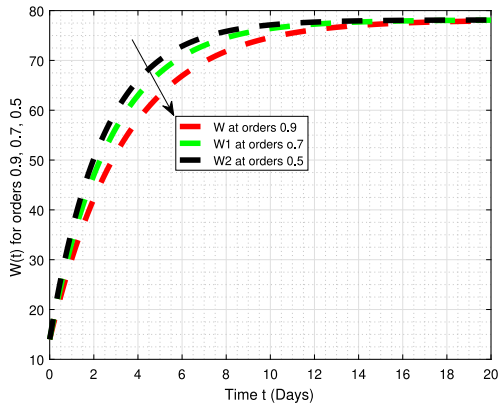

(a) Numerical illustration of the class $\mathscr{W}$ of (3.1).

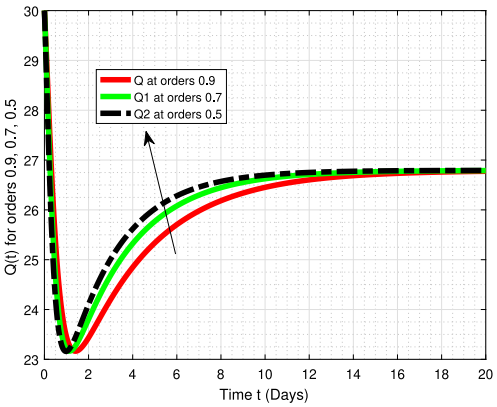

(b) Numerical illustration of the class $\mathscr{Q}$ of (3.1).

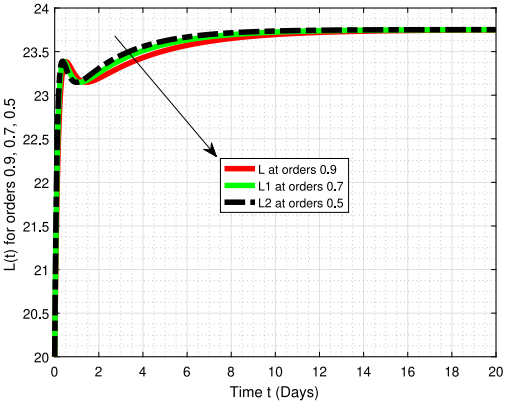

(c) Numerical illustration of the class $\mathscr{L}$ of (3.1).

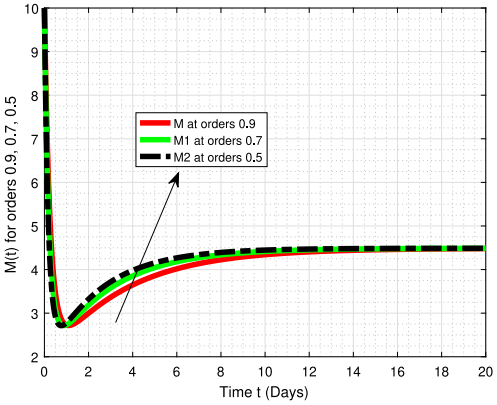

(d) Numerical illustration of the class $\mathscr{M}$ of (3.1).

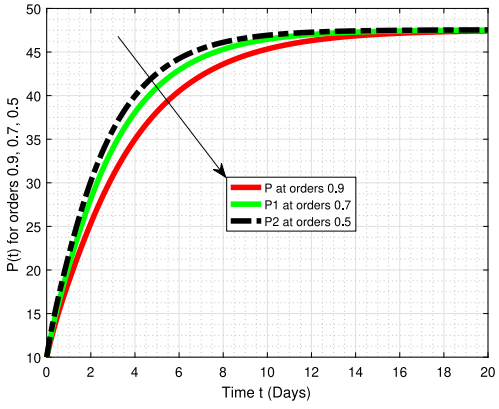

(e) Numerical illustration of the class $\mathscr{P}$ of (3.1).

Fig. 7. Graphical illustration for different fractional order of the DCOC model (3.1).

research work. Aziz Khan and Thabet Abdeljawad would like to thank Prince Sultan University for paying the support through TAS research lab.

Data availability

All data supporting this study's findings are included in the article.

References

[1] World Health Organization, Breast cancer facts, 2004, Retrived from https://www.who.int/cancer/prevention/diagnosis-screening/breast-cancer/en.
[2] S. Lei, R. Zheng, S. Zhang, W. Wei, The burden and long-term trends of breast cancer by different menopausal status in China, J. Natl. Cancer Cent. (2024).
[3] G. Pokharel, Q. Wang, M. Khan, P.J. Robson, L. Shack, K.A. Kopciuk, Stage shifting by modifying the determinants of breast cancer stage at diagnosis: A simulation study, Cancers 16 (6) (2024) 1201.
[4] CR U, Breast cancer incidence (invasive) statistics, 2020.

[5] L. Tao, Q. Wang, X. Zeng, L. Fu, J. Li, H. Chen, Psychological distress in adult women of reproductive age at different stages after breast cancer diagnosis: A qualitative study, J. Clin. Nurs. 33 (5) (2024) 1921–1932.
[6] J. Zhang, J. Deng, J. Huang, L. Mei, N. Liao, F. Yao, C. Lei, S. Sun, Y. Zhang, Monitoring response to neoadjuvant therapy for breast cancer in all treatment phases using an ultrasound deep learning model, Front. Oncol. 14 (2024) 1255618.
[7] A. Abidalkareem, A.K. Ibrahim, M. Abd, O. Rehman, H. Zhuang, Identification of gene expression in different stages of breast cancer with machine learning, Cancers 16 (10) (2024) 1864.
[8] A.S. Alnahdi, M. Idrees, Nonlinear dynamics of estrogen receptor-positive breast cancer integrating experimental data: A novel spatial modeling approach, Math. Biosci. Eng. 20 (12) (2023) 21163–21186.
[9] M. Brunetti, P. Di Giamberardino, D. Iacoviello, M. Ingrosso, Breast cancer epidemic model and optimal control, in: ICINCO, No. 2, 2023, pp. 195–202.
[10] A.M. Baba, U.C. Doko, H. Usman, M. Mamuda, U. Garba, N.M. Kontagora, Modeling breast cancer and its optimal control, Sigma Mu J. Math. Stat. Data Sci. 1 (1) (2023) 16–30.
[11] S. Benzekry, M. Mastri, C. Nicolò, J.M. Ebos, Machine-learning and mechanistic modeling of primary and metastatic breast cancer growth after neoadjuvant targeted therapy, 2023, bioRxiv 2023-02.
[12] M.S. Arshad, Z. Afzal, M.N. Aslam, F. Yasin, J.E. Macías-Díaz, A. Zarnab, Analyzing the impact of time-fractional models on chemotherapy's effect on cancer cells, Alex. Eng. J. 98 (2024) 1–9.
[13] A. Chavada, N. Pathak, S.R. Khirsariya, A fractional mathematical model for assessing cancer risk due to smoking habits, Math. Model. Control. 4 (3) (2024) 246–259.
[14] H. Mohammadpoor, N. Eghbali, L. Sajedi, M. Nosrati Sahlan, Stability analysis of fractional order breast cancer model in chemotherapy patients with cardiotoxicity by applying LADM, Adv. Contin. Discret. Model. 2024 (1) (2024) 6.
[15] K.A. Aldwoah, M.A. Almalahi, M. Hleili, F.A. Alqarni, E.S. Aly, K. Shah, Analytical study of a modified-ABC fractional order breast cancer model, J. Appl. Math. Comput. (2024) 1–32.
[16] H. Khan, T. Abdeljawad, J.F. Gómez-Aguilar, H. Tajadodi, A. Khan, Fractional order Volterra integro-differential equation with Mittag–Leffler kernel, Fractals 29 (06) (2021) 2150154.
[17] H. Khan, A.H. Rajpar, J. Alzabut, M. Aslam, S. Etemad, S. Rezapour, On a fractal–fractional-based modeling for influenza and its analytical results, Qual. Theory Dyn. Syst. 23 (2) (2024) 70.
[18] R. Jan, S. Qureshi, S. Boulaaras, V.T. Pham, E. Hincal, R. Guefaifia, Optimization of the fractional-order parameter with the error analysis for human immunodeficiency virus under Caputo operator, Discret. Contin. Dyn. Syst. S 16 (8) (2023) 2118–2140.
[19] A. Alkhazzan, J. Wang, Y. Nie, H. Khan, J. Alzabut, A novel SIRS epidemic model for two diseases incorporating treatment functions, media coverage, and three types of noise, Chaos Solitons Fractals 181 (2024) 114631.
[20] R. Jan, N.N. Razak, S. Qureshi, I. Ahmad, S. Bahram, Modeling rift valley fever transmission: insights from fractal-fractional dynamics with the Caputo derivative, Math. Model. Control. 4 (2) (2024) 163–177.
[21] R. Jan, H. Degaichia, S. Boulaaras, Z.U. Rehman, S. Bahram, Qualitative and quantitative analysis of vector-borne infection through fractional framework, Discret. Contin. Dyn. Syst. S (2024).
[22] F.M. Atici, P. Eloe, Discrete fractional calculus with the nabla operator, Electron. J. Qual. Theory Differ. Equ. [Electron. Only] 2009 (2009) Paper-No.
[23] T. Abdeljawad, D. Baleanu, Discrete fractional differences with nonsingular discrete Mittag–Leffler kernels, Adv. Difference Equ. 2016 (1) (2016) 1–22.
[24] T. Abdeljawad, On Riemann and Caputo fractional differences, Comput. Math. Appl. 62 (3) (2011) 1602–1611.
[25] J. Ran, Discrete chaos in a novel two-dimensional fractional chaotic map, Adv. Differ. Equ. 2018 (1) (2018) 294.
[26] T. Sitthiwirattham, A. Zeb, S. Chasreechai, Z. Eskandari, M. Tilioua, S. Djilali, Analysis of a discrete mathematical COVID-19 model, Results Phys. 28 (2021) 104668.
[27] M. El Karchani, N. Idrissi Fatmi, K. Mouden, Analysing the effect of trastuzumab treatment on breast cancer stages and cardiac function: A mathematical modeling and numerical simulation, Commun. Math. Biol. Neurosci. 2023 (2023) Article-ID.
[28] M. Idrees, A.S. Alnahdi, M.B. Jeelani, Mathematical modeling of breast cancer based on the Caputo–Fabrizio fractal-fractional derivative, Fractal Fract. 7 (11) (2023) 805.
[29] M. Fathoni, G. Gunardi, F.A. Kusumo, S.H. Hutajulu, Mathematical model analysis of breast cancer stages with side effects on heart in chemotherapy patients, in: AIP Conference Proceedings 2019, Vol. 2192, No. 1, AIP Publishing.
[30] G.C. Wu, D. Baleanu, Discrete fractional logistic map and its chaos, Nonlinear Dyn. 75 (2014) 283–287.
[31] A.Q. Khan, M. Tasneem, M.B. Almatrafi, Discrete-time covid-19 epidemic model with bifurcation and control, Math. Biosci. Eng. 19 (2021) 1944–1969.
[32] C. Maharajan, C. Sowmiya, C. Xu, Delay dependent complex-valued bidirectional associative memory neural networks with stochastic and impulsive effects: An exponential stability approach, Kybern. 60 (3) (2024) 317–356.
[33] V.K. Shukla, M.C. Joshi, P.K. Mishra, C. Xu, Adaptive fixed-time difference synchronization for different classes of chaotic dynamical systems, Phys. Scr. 99 (9) (2024) 095264.
[34] Y. Yang, Q. Qi, J. Hu, J. Dai, C. Yang, Adaptive fault-tolerant control for consensus of nonlinear fractional-order multi-agent systems with diffusion, Fractal Fract. 7 (10) (2023) 760.
[35] T. Jia, X. Chen, L. He, F. Zhao, J. Qiu, Finite-time synchronization of uncertain fractional-order delayed memristive neural networks via adaptive sliding mode control and its application, Fractal Fract. 6 (9) (2022) 502.
[36] R. Xing, M. Xiao, Y. Zhang, J. Qiu, Stability and Hopf bifurcation analysis of an (n+ m)-neuron double-ring neural network model with multiple time delays, J. Syst. Sci. Complex. 35 (1) (2022) 159–178.
[37] Y. Zi, Y. Wang, Positive solutions for Caputo fractional differential system with coupled boundary conditions, Adv. Differ. Equ. 2019 (2019) 1–2.
[38] Z. Liu, Y. Ding, C. Liu, C. Zhao, Existence and uniqueness of solutions for singular fractional differential equation boundary value problem with p-Laplacian, Adv. Differ. Equ. 2020 (1) (2020) 83.
[39] M.Z. Baber, M.W. Yasin, C. Xu, N. Ahmed, M.S. Iqbal, Numerical and analytical study for the stochastic spatial dependent prey–predator dynamical system, J. Comput. Nonlinear Dyn. 19 (10) (2024).
[40] X. Jiang, X. Chen, M. Chi, J. Chen, On hopf bifurcation and control for a delay systems, Appl. Math. Comput. 370 (2020) 124906.
[41] C. Jiang, A. Zada, M.T. Şenel, T. Li, Synchronization of bidirectional N-coupled fractional-order chaotic systems with ring connection based on antisymmetric structure, Adv. Differ. Equ. 2019 (1) (2019) 1–6.
[42] B. Zhang, Y. Xia, L. Zhu, H. Liu, L. Gu, Global stability of fractional order coupled systems with impulses via a graphic approach, Mathematics 7 (8) (2019) 744.